Waveguide superconducting single-photon detectors for integrated quantum photonic circuits

Waveguide superconducting single-photon detectors for integrated quantum photonic circuits

J. P. Sprengers, A. Gaggero, D. Sahin, S. Jahanmirinejad, G. Frucci et al.

Citation: Appl. Phys. Lett. **99**, 181110 (2011); doi: 10.1063/1.3657518
View online: http://dx.doi.org/10.1063/1.3657518
View Table of Contents: http://apl.aip.org/resource/1/APPLAB/v99/i18
Published by the American Institute of Physics.

Waveguide superconducting single-photon detectors for integrated quantum photonic circuits

J. P. Sprengers,[1,a)] A. Gaggero,[2,a)] D. Sahin,[1,b)] S. Jahanmirinejad,[1] G. Frucci,[1] F. Mattioli,[2] R. Leoni,[2] J. Beetz,[3] M. Lermer,[3] M. Kamp,[3] S. Höfling,[3] R. Sanjines,[4] and A. Fiore[1]
[1]*COBRA Research Institute, Eindhoven University of Technology, P. O. Box 513, Eindhoven 5600 MB, The Netherlands*
[2]*Istituto di Fotonica e Nanotecnologie, CNR, Via Cineto Romano 42, Roma 00156, Italy*
[3]*Technische Physik, Physikalisches Institut and Wilhelm Conrad Röntgen Research Center for Complex Material Systems, Universität Würzburg, Am Hubland, Würzburg D-97074, Germany*
[4]*Institute of Condensed Matter Physics, Ecole Polytechnique Fédérale de Lausanne (EPFL), Station 3, Lausanne CH-1015, Switzerland*

(Received 31 August 2011; accepted 12 October 2011; published online 1 November 2011)

The monolithic integration of single-photon sources, passive optical circuits, and single-photon detectors enables complex and scalable quantum photonic integrated circuits, for application in linear-optics quantum computing and quantum communications. Here, we demonstrate a key component of such a circuit, a waveguide single-photon detector. Our detectors, based on superconducting nanowires on GaAs ridge waveguides, provide high efficiency (~20%) at telecom wavelengths, high timing accuracy (~60 ps), and response time in the ns range and are fully compatible with the integration of single-photon sources, passive networks, and modulators. © *2011 American Institute of Physics*. [doi:10.1063/1.3657518]

The combination of single-photon sources, passive optical circuits, and single-photon detectors enables important functionalities in quantum communications, such as quantum repeaters[1] and qubit amplifiers,[2] and also forms the basis of all-optical quantum gates[3] and of linear-optics quantum computing.[4] However, present implementations are limited to few qubits, due to the large number of optical components required and the corresponding complexity and cost of experimental set-ups. The monolithic integration of quantum photonic components and circuits on a chip is absolutely required to scale implementations of optical quantum information processing to meaningful numbers of qubits. The integration of passive circuits has been demonstrated in waveguides based on silica-on-silicon[5] and on laser-micromachined glass,[6,7] but a platform for the simultaneous integration of sources, detectors, and passive circuitry is still missing. The integration of detectors is particularly challenging, as the complex device structures associated to avalanche photodiodes are not easily compatible with the integration with low-loss waveguides and even less with sources. Transition-edge sensors may be suited for integration,[8] but they are plagued by very slow response times (leading to maximum counting rates in the tens of kHz range) and require cooling down to <100 mK temperatures. Here, we report a simple approach to the realization of single-photon detectors on optical waveguides in the GaAs/AlGaAs material system. It enables the demonstration of efficient waveguide single-photon detectors (WSPDs) with response times in the ns range and is fully compatible with the integration of sources and passive optical circuits on a single chip.

Our WSPDs are based on the principle of photon-induced hot-spot creation in ultranarrow superconducting NbN wires, which is also used in nanowire superconducting single-photon detectors (SSPDs)[9] and can provide ultrahigh sensitivity at telecommunication wavelengths, high counting rates, broad spectral response, and high temporal resolution due to low jitter values. In our design (see Fig. 1), the wires are deposited and patterned on top of a GaAs ridge waveguide, in order to sense the evanescent field on the surface. Four NbN nanowires (4 nm-thick, 100 nm wide, and spaced by 150 nm) are placed on top of a GaAs (300 nm)/$Al_{0.75}Ga_{0.25}As$ waveguide, and a 1.85 μm-wide, 250 nm-deep ridge is etched to provide 2D confinement. We assume that a 100 nm-thick SiO_x layer is left on top of the wires as a residue of the hydrogen silsesquioxane (HSQ) mask used for

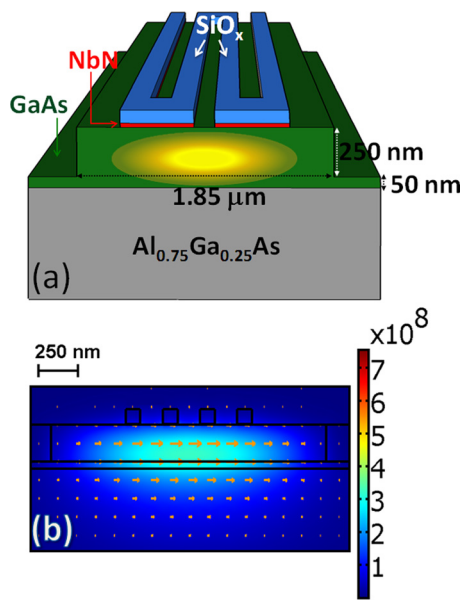

FIG. 1. (Color online) (a) Schematic view and (b) Contour and vector plot of the amplitude [V/m] and direction of the electric field for the fundamental mode ($\lambda = 1300$ nm) of the waveguide superconducting single-photon detector.

[a)]J. P. Sprengers and A. Gaggero contributed equally to this work.
[b)]Electronic mail: d.sahin@tue.nl.

patterning the wires. The dimensions of the waveguide have been optimized to obtain maximum absorption by the NbN wires while leaving a 0.5 μm alignment margin between the wires and the side of the ridge. The electric field amplitude and polarization for the fundamental mode, calculated using a finite-element mode solver (COMSOL Multiphysics), is shown in Fig. 1(b) for $\lambda = 1300$ nm. For this quasi-transverse-electric (TE) mode, we calculate a modal absorption coefficient of $\alpha_{abs} = 451\ cm^{-1}$ (assuming a refractive index of 5.23–5.82i (Ref. 10) for NbN), corresponding to 90% (99%) absorptance after 51 μm (102 μm) propagation length. This very high and broadband absorptance in an ultrathin wire is unique to waveguide geometries, which allow an interaction length limited only by extrinsic waveguide losses. Since the NbN wires produce a very small perturbation to the guided mode, the impedance mismatch at the interface between the passive waveguide without wires and the detecting section is negligible (calculated modal reflectivity of 5.84×10^{-5}%), allowing very efficient coupling to the detector. We note that this design with a TE-polarized, tightly confined mode is optimized for on-chip applications with integrated single-photon sources (quantum dots in waveguides), which emit in the TE polarization. In contrast, transverse magnetic (TM) polarized modes have a complex spatial profile, which makes the fiber coupling inefficient. By increasing the waveguide thickness by 50 nm, well-confined TM modes with high modal absorption coefficients $>500\ cm^{-1}$ can be obtained. The absorptance of both TE and TM light would then approach 100%, resulting in a polarization-independent quantum efficiency (QE).

Nanowire WSPDs were fabricated on top of a GaAs (300 nm)/$Al_{0.75}Ga_{0.25}As$ (1.5 μm) heterostructure grown by molecular beam epitaxy on an undoped GaAs (001) substrate. A 4.3 nm-thick NbN layer was deposited by dc reactive magnetron sputtering of a Nb target in a N_2/Ar plasma at 350 °C, with deposition parameters optimized for GaAs substrates,[11] resulting in a critical temperature $T_c = 10.0$ K, and a transition width $\Delta T_c = 650$ mK. WSPDs were then fabricated using four steps of direct-writing 100 kV electron beam lithography (EBL). In the first step, Ti(10 nm)/Au(60 nm) contact pads (patterned as a 50 Ω coplanar transmission line) and alignment markers are defined by lift-off using a PMMA mask (Fig. 2(a)). In the second step, the meander pattern is defined on a 180 nm thick (HSQ) mask and then transferred to the NbN film with a (CHF_3+SF_6+Ar) reactive ion etching (RIE). Fig. 2(b) shows a scanning electron microscopy (SEM) image of an etched wire. The meandered NbN nanowire (100 nm width, 250 nm pitch, and 30-100 μm length), still covered with the HSQ mask, is very regular with a width uniformity of about 5%. In the third step, an HSQ-mask for the waveguide patterning is defined by carefully realigning this layer with the previous one. This layer also protects the Ti/Au pads against the subsequent reactive etching process. Fig. 2(c) shows an atomic force microscopy (AFM) image of the waveguide etch mask aligned to the wires, showing realignment accuracy better than 100 nm (Fig. 2(d)). Successively, 250 nm of the underlying GaAs layer is etched by a Cl_2+Ar ECR (electron cyclotron resonance) RIE. Finally, in order to allow the electrical wiring to the TiAu pads, vias through the remaining HSQ-mask are opened using a PMMA mask and RIE in a CHF_3 plasma.

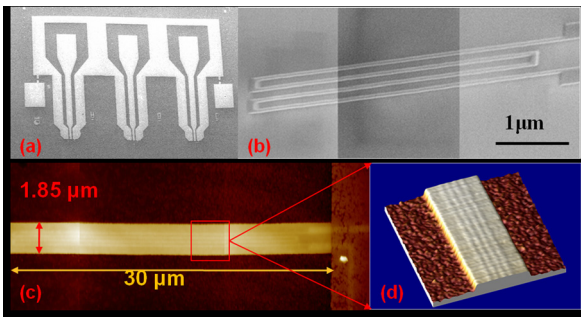

FIG. 2. (Color online) (a) Scanning electron microscope (SEM) micrograph of Ti/Au electric contacts; (b) Collection of three SEM micrographs taken in different regions of a 30 μm long WSPD, the nanowires are still covered by the HSQ etching mask; (c) Atomic force microscope (AFM) image of the 1.85 μm wide and 30 μm long HSQ mask used for the etching of the waveguide aligned on top of the NbN nanowires; and d) AFM Enlarged view of the waveguide HSQ etching mask showing a realignment accuracy better than 100 nm.

The waveguides were cleaved leaving a 1 mm-long passive ridge waveguide between the cleaved facet and the WSPD.

The WSPDs were characterized by end-fire coupling light from a polarization-maintaining lensed fiber (producing a spot with nominal diameter of 2.5 ± 0.5 μm) into the waveguides mounted on the cold finger of a continuous flow helium cryostat. Both the lensed fiber and the contact probes are mounted on piezoelectric positioners, which are thermally anchored to the cold plate to minimize the thermal load to the detector, resulting in an operating temperature <4 K. The inset of Fig. 3 displays the current-voltage characteristic measured for a 50 μm-long WSPD, showing a critical current (I_c) of 16.9 μA. The electro-optical response was measured by end-fire coupling a continuous wave 1300 nm diode laser through the lensed fiber in the TE polarization. The detector count rate was observed to be extremely sensitive to the fiber-waveguide alignment and to their distance, confirming that the detector responds to guided photons and not to stray light propagating along the surface or in the substrate. The count rate was measured to be proportional to the laser power (Fig. 3), proving operation in the single-photon regime. The inset in Fig. 4 shows a single WSPD output pulse, showing a pulse duration (full-width-half-maximum) of 3.2 ns and a 1/e decay time of 3.6 ns, which corresponds very well to the expected time constant $\tau = L_{kin}/R = 3.6$ ns, where $L_{kin} = 180$ nH is the wire kinetic inductance (as calculated from the kinetic inductance per square for similar NbN wires, L = 90 pH/□ (Ref. 12))

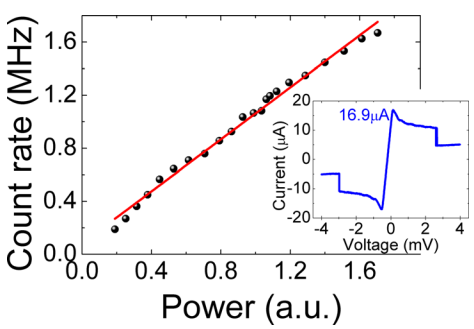

FIG. 3. (Color online) Count rate as a function of laser power ($\lambda = 1300$ nm, TE polarization, $I_b = 9.9$ μA), showing a linear behavior and hence operation in the single-photon regime. Inset: Current-voltage characteristic of the WSPD, showing a critical current of 16.9 μA, the relaxation-oscillation region, and the beginning of the hot-spot plateau.

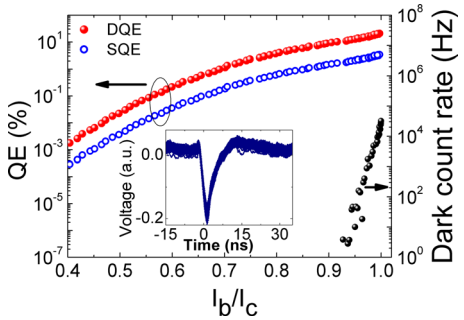

FIG. 4. (Color online) Device QE (open symbols) and system QE (closed symbols) of a 50 μm-long WSPD under illumination at 1300 nm in the TE polarization (left axis) and dark count rate (black dots, right axis) as a function of the normalized bias current. Inset: WSPD output pulse after 48 dB amplification.

and $R = 50\ \Omega$ is the load resistance. Considering that it takes a time $\approx 3\tau$ to recover 95% of the bias current after detection, we estimate a maximum counting rate close to 100 MHz. By illuminating the device with a pulsed diode laser, a total jitter of 73 ps was measured on the WSPD output pulse, corresponding to a 61 ps intrinsic detector jitter after correcting for the 40 ps jitter from the laser pulse.

The measured QE (1300 nm, TE polarization) is plotted in Fig. 4 (left axis) as a function of the normalized bias current I_b/I_c. The system quantum efficiency (SQE, open symbols), defined as the number of counts divided by the average photon number in the fiber at the input of the cryostat, reaches 3.4% for a 50 μm-long device. For determining the number of photons coupled into the waveguide, transmission measurements were performed with a tunable laser on a sample containing 3 mm-long ridge waveguides, but without NbN wires and contact pads. From the measured Fabry-Perot fringes, and particularly from the maximum and minimum transmission (in TE polarization), $T_{max} = 6.1\%$ and $T_{min} = 1.8\%$, we deduce that the propagation loss over a 3 mm waveguide length is negligible. Assuming symmetric input/output coupling and using the standard expression for the Fabry-Perot transmission,[13] we derive a coupling efficiency (from fiber input) of 17.4%. The corresponding device quantum efficiency (DQE), defined with respect to the number of photons coupled to the waveguide, is plotted as closed symbols in Fig. 4 and reaches 19.7%. This value is still lower than the calculated absorptance (90% in the 50 μm-long WSPD), which we mainly attribute to a limited internal quantum efficiency (detection probability upon absorption of a photon), and further improvements of film quality and wire etching process may result in notably improved values. Another potential cause for limited efficiency may be extrinsic loss (e.g., scattering) due to the nanowires, which is however believed to be small as compared to nanowire absorption. The dark count rate was measured in another cryostat without optical windows at 1.2 K and is presented in Fig. 4 (right axis), showing the usual exponential dependence as a function of the bias current.

In conclusion, we have demonstrated integrated waveguide single-photon detectors based on superconducting nanowires on GaAs ridge waveguides. They provide system (device) quantum efficiencies of 3.4% (≈20%) at 1300 nm, a timing resolution ~60 ps, and dead times of few ns. Further optimization of film deposition and device fabrication may result in efficiencies approaching 100% due to the high absorptance allowed by the waveguide geometry. Higher system QE and polarization-independence can be obtained by a waveguide design providing a more extended and symmetric mode profile and by integrating a tapered coupler.[14] Integrated photon-correlation devices[15] and photon-number-resolving detectors[16] are straightforward to realize by integrating several wires on the same waveguide. Furthermore, this technology is fully compatible with the fabrication of passive quantum circuits on GaAs waveguides, and with single-photon sources based on InAs quantum dots in waveguides, and, therefore, opens the way to fully integrated quantum photonic circuits including sources and detectors.

Note added in proof: Two alternative approaches to waveguide single-photon detection, based on transition edge sensors[8] and on superconducting nanowires on Si/SiO_2 waveguides,[17] have been reported during the submission process of this manuscript.

We acknowledge the contribution of D. Bitauld in an initial stage of this work and interesting discussions with M. Thompson and J. L. O'Brien. This work was supported by the European Commission through FP7 QUANTIP (Contract No. 244026) and Q-ESSENCE (Contract No. 248095) and by Dutch Technology Foundation STW, applied science division of NWO, the Technology Program of the Ministry of Economic Affairs.

[1]N. Sangouard, C. Simon, J. Minář, H. Zbinden, H. de Riedmatten, and N. Gisin, Phys. Rev. A **76**, 050301(R) (2007).
[2]N. Gisin, S. Pironio, and N. Sangouard, Phys. Rev. Lett. **105**, 070501 (2010).
[3]J. L. O'Brien, G. J. Pryde, A. G. White, T. C. Ralph, and D. Branning, Nature **426**, 264 (2003).
[4]E. Knill, R. Laflamme, and G. J. Milburn, Nature **409**, 46 (2001).
[5]A. Politi, M. J. Cryan, J. G. Rarity, S. Yu, and J. L. O'Brien, Science **320**, 646 (2008).
[6]G. D. Marshall, A. Politi, J. C. F. Matthews, P. Dekker, M. Ams, M. J. Withford, and J. L. O'Brien, Opt. Express **17**, 12546 (2009).
[7]L. Sansoni, F. Sciarrino, G. Vallone, P. Mataloni, A. Crespi, R. Ramponi, and R. Osellame, Phys. Rev. Lett. **105**, 200503 (2010).
[8]T. Gerrits, N. Thomas-Peter, J. C. Gates, A. E. Lita, B. J. Metcalf, B. Calkins, N. A. Tomlin, A. E. Fox, A. L. Linares, J. B. Spring, N. K. Langford, R. P. Mirin, P. G. R. Smith, I. A. Walmsley, and S. W. Nam, e-print arXiv:1107.5557v1 [quantum-ph] (2011).
[9]G. N. Gol'tsman, O. Okunev, G. Chulkova, A. Lipatov, A. Semenov, K. Smirnov, B. Voronov, A. Dzardanov, C. Williams, and R. Sobolewski, Appl. Phys. Lett. **79**(6), 705 (2001).
[10]V. Anant, A. J. Kerman, E. A. Dauler, J. K. W. Yang, K. M. Rosfjord, and K. K. Berggren, Opt. Express **16**, 10750 (2008).
[11]A. Gaggero, S. Jahanmiri Nejad, F. Marsili, F. Mattioli, R. Leoni, D. Bitauld, D. Sahin, G. J. Hamhuis, R. Nötzel, R. Sanjines, and A. Fiore, Appl. Phys. Lett. **97**, 151108 (2010).
[12]F. Marsili, D. Bitauld, A. Gaggero, S. Jahanmirinejad, R. Leoni, F. Mattioli, and A. Fiore, New J. Phys. **11**, 045022 (2009).
[13]B. E. A. Saleh and M. C. Teich, *"Fundamentals of Photonics"* (Wiley, New York, 1991), chap. 9.
[14]X. Hu, C. W. Holzwarth, D. Masciarelli, E. A. Dauler, and, K. K. Berggren, IEEE Trans. Appl. Supercond. **19**, 336 (2009).
[15]E. A. Dauler, B. S. Robinson, A. J. Kerman, J. K. W. Yang, K. Rosfjord, V. Anant, B. Voronov, G. Gol'tsman, and K. K. Berggren, IEEE Trans. Appl. Supercond. **17**, 279 (2007).
[16]A. Divochiy, F. Marsili, D. Bitauld, A. Gaggero, R. Leoni, F. Mattioli, A. Korneev, V. Seleznev, N. Kaurova, O. Minaeva, G. Gol'tsman, K. G. Lagoudakis, M. Benkhaoul, F. Lévy, and A. Fiore, Nature Photon. **2**, 302 (2008).
[17]W. H. P. Pernice, C. Schuck, O. Minaeva, M. Li, G. N. Gol'tsman, A. V. Sergienko, H. X. Tang, e-print arXiv:1108.5299v1 [physics.optics] (2011).